Stable Open-Loop Brachiation on a Vertical Wall

Nelson Rosa Jr., Adam Barber, Robert D. Gregg, and Kevin M. Lynch

Abstract— **This paper presents a hybrid mechanical model for the Gibbot, a robot that dynamically locomotes along a vertical wall in a manner analogous to gibbons swinging between branches in the forest canopy. We focus on one particular gait, continuous-contact brachiation, which always has one handhold in contact with the wall. We use zero-cost, unstable solutions corresponding to horizontal brachiation, originally found by Gomes and Ruina, as templates to generate open-loop stable gaits in arbitrary directions. The first case considered is passive brachiation down a shallow slope, roughly corresponding to upside-down locomotion of the well-studied compass-gait biped. We then consider underactuated brachiation with a constant forcing term at the elbow to produce open-loop stable descending and ascending gaits.**

I. Introduction

This paper introduces the Gibbot, a dynamic climbing robot developed for experimental validation of estimation and control of hybrid mechanical locomotion systems. The Gibbot locomotes on a vertical wall and consists of two links, each equipped with a "hand," and a single powered rotary joint connecting the two links. A hand can clamp to the wall at any time, with the link freely pivoting about the clamp. The robot locomotes by actuating the joint motor and switching between four dynamic regimes: one hand clamped, the other hand clamped, both hands free (free flight), or both hands clamped (rendering the Gibbot stationary). Our Gibbot prototype climbs on a steel wall, so we use electromagnets mounted in rotary bearings to implement the hand clamping mechanism. Due to the availability of "handholds" at any location on the wall, the Gibbot is capable of a wide variety of gaits, each consisting of a cyclic sequence of transitions among these regimes.

In this paper we focus on one particular gait of the Gibbot: continuous-contact brachiation (Figure 1). Brachiation is the style of locomotion employed by gibbons (from which the Gibbot draws its name) as they gracefully locomote through the forest canopy by swinging between branches. Fukuda and colleagues introduced brachiation to robotics by building a series of robots demonstrating the ability to swing from handhold to handhold in gravity [1]–[3]. The earliest brachiating robots consisted of two links with grippers and a single powered rotary joint, similar to the Gibbot in this paper, while later versions consisted of many degrees of freedom to better approximate the articulation of a gibbon.

The Gibbot differs from hybrid systems such as the brachiation robots of Fukuda et al., as well as walking robots, in that regime jumps can be implemented at arbitrary states. This ability to activate and deactivate the clamps at any time allows the exploration of a wide variety of gaits without the need for precisely placed handholds.

A. Statement of Contributions

This paper introduces the design of the Gibbot and demonstrates its operation. We then focus on brachiation by the Gibbot, motivated by the observation by Gomes and Ruina that zero-energy horizontal brachiation is theoretically possible [4]. They showed that, for certain initial rest configurations of the two-joint robot, and assuming zero damping or friction, the swing-through hand reaches a horizontal line of handholds with the robot at zero velocity and in a mirrored configuration of the original. This allows the robot to release one hand and clamp the other, which requires zero work, and resume swinging.

These fixed-point solutions of the dynamics consume zero energy, but they are unstable and apply only to horizontal locomotion. Using these motions as templates, in this paper we extend these solutions to "nearby" *stable* brachiation gaits:

- **Unactuated downhill brachiation.** We show the existence of stable downhill brachiation solutions without powering the motor. The swing-through hand clamps on the downhill slope at nonzero velocity, causing an energy-dissipating impact. Potential energy due to gravity restores the kinetic energy by the end of the next swing, resulting in a fixed point in the dynamics. For some slopes, these fixed points are shown to be stable. The passive brachiator is roughly analogous to an upside-down passive compass gait walker [5], [6], but the brachiator has gaits with much larger domains of attraction.
- **Open-loop brachiation in arbitrary directions.** We show the existence of stable powered brachiation gaits without the use of feedback. Certain choices of swing-through duration and actuator torques lead to stable fixed points corresponding to horizontal brachiation, uphill brachiation, and downhill brachiation.

This general strategy of morphing unstable passive dynamic motions into powered but stable motions leads naturally to graceful locomotion, typically with a trade-off between stability and efficiency.

N. Rosa and A. Barber are with the Department of Mechanical Engineering, and K.M. Lynch is with the Department of Mechanical Engineering and the Northwestern Institute on Complex Systems, Northwestern University, Evanston, IL 60208. R.D. Gregg is with the Center for Bionic Medicine, Rehabilitation Institute of Chicago, Chicago, IL 60611. {nelsonrosa2013,adam.barber}@u.northwestern.edu, {rgregg,kmlynch}@northwestern.edu

This work was supported by NSF grants IIS-0803734 and IIS-1018167.

Fig. 1: The Gibbot executing a single brachiation swing on a steel wall.

B. Related Work

The work reported in this paper has two main inspirations: the brachiation robots of [1]–[3] and the theoretical zero-energy horizontal brachiation of [4]. Brachiation on isolated handholds is achieved by feedback control in [1]–[3], while our focus is on unactuated and open-loop control. Unstable zero-energy brachiation is studied in [4]; in this paper, we focus on nearby energy-efficient but stable brachiation gaits.

The approach of using zero-energy locomotion solutions as templates for controlled solutions has been employed by Ruina et al. for nearly-passive controlled walking on flat ground [7] and Spong et al. for walking on varying slopes [8] and in 3D spaces [9].

Other robots which share a family resemblance to the Gibbot are the two-link robot of Bullo and Žefran [10], the Acrobot [11], the ROCR robot of Provancher et al. [12], and the bridge inspection robot of Mazumdar and Asada [13]. The two-link hybrid robot described in simulation in [10] locomotes on a horizontal plane by switching between sliding, clamped, and rolling modes, and is used to demonstrate controllability properties of hybrid mechanical systems. When the Gibbot has a single hand clamped, it becomes the Acrobot [11], a double pendulum with an actuator at the middle joint. The use of clamping and dynamic swinging motions for climbing locomotion is also employed in ROCR, which uses claws to grasp a textured wall [12]. The bridge inspection robot in [13] uses intermittent brachiation-style swinging motions to "step over" obstacles on the underside of a bridge, but the robot must come to rest between steps.

The Gibbot's hand clamping mechanism uses an electromagnet mounted in rotary bearings. This choice was made for design simplicity and fast activation/deactivation of the clamps, but not for power efficiency. Another option for activating and deactivating a clamp is to mechanically rotate a permanent magnet [13], [14], which has the advantage that no power is needed to maintain the clamp indefinitely, at the possible cost of speed of attachment and detachment.

C. Paper Outline

We begin in Section II by describing the design and operation of the Gibbot. Section III provides a mathematical model of the hybrid mechanical system and summarizes the results of Gomes and Ruina [4]. Section IV examines passive downhill brachiation, and Section V addresses open-loop stable powered brachiation on arbitrary slopes. We conclude in Section VII with remarks and future work.

II. Gibbot Design and Operation

The Gibbot began as an undergraduate mechatronics project and has evolved to the current design, built in collaboration with Kinea Design, LLC (Figure 2). The robot locomotes on a vertical steel sheet by switching its two electromagnets on and off and powering the motor at its middle joint. A geared 19.5:1 GM8224 Pittman motor with a 500 line encoder powers the elbow joint. An additional 3:1 bevel gearing allows the motor to lay flat along one link and brings the maximum output torque at the joint to approximately 6 Nm. The electronics of the robot consist of an onboard PIC32 running at 80 MHz with an XBee chip for wireless communication. In addition to the motor encoder, the Gibbot is outfitted with two rotary encoders mounted over the magnets, as well as gyros and accelerometers on each link to measure the angular velocity and acceleration of the arms. Three LEDs are visible to an external high-speed camera, allowing real-time feedback control over the wireless XBee link. The entire robot is powered by two 11.1 V Lithium-ion batteries. The total weight of the robot is about 2.36 kg.

Fig. 2: (Top) Perspective view of the Gibbot. (Bottom) A view of the underside of the Gibbot.

We have included a supplementary video of the Gibbot in motion available at http://ieeexplore.ieee.org.

III. The Hybrid Dynamics

Notation for the Gibbot is shown in Figure 3. The configuration vector is written $q = [q_1, q_2, q_3, q_4]^T$, where (q_1, q_2) are the x-y coordinates of hand 1 in a world frame, q_3 is the

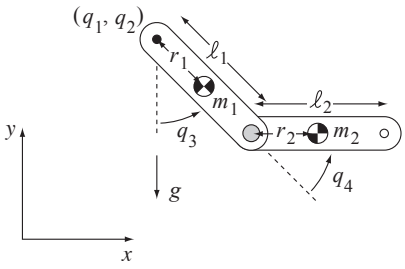

Fig. 3: The Gibbot model.

Magnet State	Magnet 1	Magnet 2	Dynamics
0	0	0	Free Flight
1	0	1	Double Pendulum
2	1	0	Double Pendulum
3	1	1	At Rest

TABLE I: Four magnet states and corresponding motions.

angle of link 1 from the vertical, and q_4 is the angle of link 2 from link 1. The lengths of the two links from the hands to the motor are ℓ_1 and ℓ_2, and r_1 and r_2 are the distances from the hand to the center of mass of link 1 and from the motor to the center of mass of link 2, respectively. The mass and inertia of the links about their center of mass are m_i and I_i.

The Gibbot is a hybrid mechanical system described by four different dynamic regimes (free flight, hand 1 clamped, hand 2 clamped, or both hands clamped) depending on the on-off state of the two magnets. We represent the magnet state as $b \in \{0, 1, 2, 3\}$ (Table I). Two of these regimes correspond to double pendulum dynamics, so we collapse them into one in the finite state machine of Figure 4. The hybrid dynamics consists of periods of motion within a regime punctuated by transitions between regimes, which may result in instantaneous change of the Gibbot velocity. Defining $x = [q^T, \dot{q}^T]^T$ as the state of the system, a transition between regimes is represented by

$$x^+ = H_{b^+}(x^-),$$

where x^- is the pre-transition state, x^+ is the post-transition state, and b^+ is the post-transition regime. Thus there are four transition maps, H_0 through H_3, depending on the hand state after the jump.

Below we give the continuous dynamics within the regimes, then the transition maps due to changing magnet states, and finally define fixed points of the hybrid dynamics and the zero-energy fixed points discovered by Gomes and Ruina.

A. The Continuous Dynamics

We nondimensionalize the dynamics such that time is scaled by $d_t = \sqrt{\frac{\ell_1+\ell_2}{g}}$, lengths are scaled by $d_\ell = \ell_1 + \ell_2$, and torques are scaled by $d_u = g m_2 r_2$. This results in the following set of nondimensionalized parameters used in this section:

$$\begin{aligned}
&\alpha = d_\ell \tfrac{m_1+m_2}{m_2 r_2} && \beta = \tfrac{m_1 r_1 + m_2 \ell_1}{m_2 r_2} \\
&\delta_1 = \tfrac{\ell_1}{d_\ell} && \delta_2 = \tfrac{\ell_2}{d_\ell} \\
&\gamma = \tfrac{g d_t^2}{d_\ell} && \kappa_1 = \tfrac{1}{d_\ell}\left(\tfrac{I_2}{m_2 r_2} + r_2\right) \\
&\kappa_2 = \tfrac{1}{d_\ell}\left(\tfrac{I_1 + m_1 r_1^2}{m_2 r_2} + \tfrac{\ell_1^2}{r_2}\right)
\end{aligned}$$

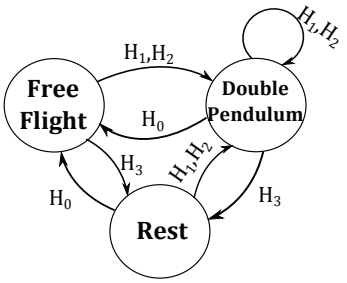

Fig. 4: The hybrid dynamics as a finite state machine.

1) The Free Flight Dynamics, Regime 0: If both magnets are off, then the robot is in free flight and the equations of motion are

$$\dot{x} = \begin{bmatrix} \dot{q} \\ M_0^{-1}(q)(U_0 - C_0(q,\dot{q})\dot{q} - G_0(q)) \end{bmatrix}, \tag{1}$$

where U_0 is the control vector, M_0 is the inertia matrix, C_0 is the Coriolis matrix, and G_0 is the gravitational vector:

$$\begin{aligned}
U_0 &= \gamma \begin{bmatrix} 0 \\ 0 \\ 0 \\ u \end{bmatrix} \\
M_0(q) &= \begin{bmatrix} \alpha & 0 & \beta c_3 + c_{34} & c_{34} \\ 0 & \alpha & \beta s_3 + s_{34} & s_{34} \\ \beta c_3 + c_{34} & \beta s_3 + s_{34} & \kappa_1 + \kappa_2 + 2\delta_1 c_4 & \kappa_1 + \delta_1 c_4 \\ c_{34} & s_{34} & \kappa_1 + \delta_1 c_4 & \kappa_1 \end{bmatrix} \\
C_0(q,\dot{q}) &= \begin{bmatrix} 0 & 0 & -(\beta s_3 \dot{q}_3 + s_{34}(\dot{q}_3 + \dot{q}_4)) & -s_{34}(\dot{q}_3 + \dot{q}_4) \\ 0 & 0 & \beta c_3 \dot{q}_3 + c_{34}(\dot{q}_3 + \dot{q}_4) & c_{34}(\dot{q}_3 + \dot{q}_4) \\ 0 & 0 & -\delta_1 s_4 \dot{q}_4 & -\delta_1 s_4 (\dot{q}_3 + \dot{q}_4) \\ 0 & 0 & \delta_1 s_4 \dot{q}_3 & 0 \end{bmatrix} \\
G_0(q) &= \gamma \begin{bmatrix} 0 \\ \alpha \\ \beta s_3 + s_{34} \\ s_{34} \end{bmatrix}.
\end{aligned} \tag{2}$$

We use the short-hand notation c_{34} to denote $\cos(q_3 + q_4)$ and similarly for the sine function.

2) The Double Pendulum Dynamics, Regimes 1 and 2: If only one magnet is on, then the Gibbot swings like a double pendulum. Defining (q_1, q_2) to be the pivot point, we focus on a reduced set of coordinates (q_3, q_4), known as the shape variables. Defining $\theta = [q_3, q_4]^T$, the reduced set of equations are

$$\ddot{\theta} = M_1(\theta)^{-1}(U_1 - C_1(\theta,\dot{\theta})\dot{\theta} - G_1(\theta)), \tag{3}$$

where

$$\begin{aligned}
U_1 &= \gamma \begin{bmatrix} 0 \\ u \end{bmatrix} \\
M_1(\theta) &= \begin{bmatrix} \kappa_1 + \kappa_2 + 2\delta_1 c_4 & \kappa_1 + \delta_1 c_4 \\ \kappa_1 + \delta_1 c_4 & \kappa_1 \end{bmatrix} \\
C_1(\theta,\dot{\theta}) &= \begin{bmatrix} -\delta_1 s_4 \dot{q}_4 & -\delta_1 s_4 (\dot{q}_3 + \dot{q}_4) \\ \delta_1 s_4 \dot{q}_3 & 0 \end{bmatrix} \\
G_1(\theta) &= \gamma \begin{bmatrix} \beta s_3 + s_{34} \\ s_{34} \end{bmatrix}.
\end{aligned} \tag{4}$$

3) The Rest Dynamics, Regime 3: When both magnets are on the robot cannot move, i.e., $\dot{x} = 0$.

B. The Transition Maps

In order for the robot to transition from one regime into the next, it has to change its magnet state. This may cause a jump in the velocity of the system. We capture this behavior with a transition map that sends the robot's state into a different dynamic regime. The transition map depends only on the new regime b^+.

1) Transition to the Double Pendulum: When the robot transitions from free flight into double pendulum mode, or from one double pendulum mode to the other, the robot undergoes an impact at the magnet that turns on. This causes a jump in the velocity of the system.

We can relate the pre-impact velocities to the post-impact velocities using impulse and conservation equations, which give us an impact map $P(q)$. We assume that the impact is plastic, instantaneous, and that non-impulsive forces are negligible. This leads to the following set of equations:

$$q^+ = q^- \tag{5}$$

$$J(q^-)\dot{q}^+ = 0 \tag{6}$$

$$M(q^-)(\dot{q}^+ - \dot{q}^-) = J^T(q^-)\,\Pi \tag{7}$$

where the $+$ and $-$ superscripts represent the pre- and post-impact variables, $M(q)$ is the mass matrix from the free flight dynamics, Π is the 2×1 impulse vector, and $J(q)$ is the Jacobian satisfying $\dot{p} = J(q)\dot{q}$, where $\dot{p}$ is the linear velocity of the hand about to clamp. The first two equations are the instantaneous and plastic impact assumptions, while the third equation is the impulse and conservation equations in generalized coordinates. We now derive an expression for $P(q)$ by first rewriting (7) as

$$\dot{q}^+ = M^{-1}J^T\Pi + \dot{q}^-. \tag{8}$$

Substituting into (6) and rearranging terms, we get

$$\Pi = -\left(JM^{-1}J^T\right)^{-1} J\dot{q}^-.$$

Plugging the results back into (8), we arrive at

$$\dot{q}^+ = \left(I - M^{-1}J^T\left(JM^{-1}J^T\right)^{-1}J\right)\dot{q}^-$$

and define $P(q)$ as

$$P(q) = I - M(q)^{-1}J^T(q)\left(J(q)M(q)^{-1}J^T(q)\right)^{-1}J(q). \tag{9}$$

Depending on which magnet is about to clamp, $J(q)$ can take one of two possible forms,

$$J_1(q) = \begin{bmatrix} 1 & 0 & 0 & 0 \\ 0 & 1 & 0 & 0 \end{bmatrix} \tag{10}$$

or

$$J_2(q) = \begin{bmatrix} 1 & 0 & \delta_1 c_3 + \delta_2 c_{34} & \delta_2 c_{34} \\ 0 & 1 & \delta_1 s_3 + \delta_2 s_{34} & \delta_2 s_{34} \end{bmatrix}. \tag{11}$$

We want to retain the same double pendulum dynamics regardless of whether J equals J_1 or J_2, so there will be times when we need to redefine coordinates (i.e., which hand location is identified with (q_1, q_2)). We will write the jump map in such a way that the post-impact velocities are correct regardless of whether or not the coordinate system has to be flipped. Let

$$A(q) = \begin{bmatrix} q_1 + \delta_1 s_3 + \delta_2 s_{34} \\ q_2 - \delta_1 c_3 - \delta_2 c_{34} \\ \pi + q_3 + q_4 \\ -q_4 \end{bmatrix}, \tag{12}$$

which we will invoke whenever we need to flip the coordinate system. We also assume that the physical parameters and the labels for each link are swapped as well. Then the transition map is written

$$x^+ = H_i(x^-) = \begin{cases} \begin{bmatrix} q^- \\ P(q^-)\dot{q}^- \end{bmatrix}, & J = J_1 \\ \\ \begin{bmatrix} A(q^-) \\ \frac{\partial A(q)}{\partial q}(q^-)P(q^-)\dot{q}^- \end{bmatrix}, & J = J_2 \end{cases} \tag{13}$$

for $i = 1, 2$.

2) Transition to Free Flight: Because there are no impulsive forces, the transition map is $x^+ = H_0(x^-) = x^-$.

3) Transition to Rest: When both magnets are activated the Gibbot becomes immobile, so we have

$$x^+ = H_3(x^-) = \begin{bmatrix} I & 0 \\ 0 & 0 \end{bmatrix} x^-. \tag{14}$$

C. Definition of a Brachiation Fixed Point

To draw a connection to the results of Gomes and Ruina, for the rest of the paper we assume the Gibbot is symmetric, so all masses, lengths, etc. of the two links are identical.

If we let b^+, b^- represent the pre- and post-impact magnet states, F_0, F_1, F_3 be the equations of motion of the free flight dynamics, double pendulum, and rest dynamics, respectively, and let $F_2 = F_1$ (by the symmetry of the Gibbot), then we can write the dynamics from one post-transition state to the next as

$$x^+ = H_{b^+}(x^-) = H_{b^+}\left(x_0 + \int_0^T F_{b^-}(x(s), u(s))\,ds\right) \tag{15}$$

and explicitly show the dependence on initial conditions x_0, forcing function $u(t)$, switching time T, and magnet states b^+ and b^-. Defining λ as the collection of the switch time T, the new magnet state b^+, and the control function $u(t)$, we can write (15) as $x^+ = \mathcal{H}(x_0, \lambda)$. If we restrict the robot's locomotion so that it is never in free flight, then we can define a return map S on the shape space with reduced state vector $x_\theta = [\theta^T, \dot{\theta}^T]^T$,

$$x_\theta^1 = S\left(x_\theta^0, \lambda^0\right). \tag{16}$$

Since the robot cannot be in free flight, the shape variables and their derivatives are sufficient to define a fixed point of the system corresponding to period-one cyclic motion, i.e.,

$$x_\theta^* = S\left(x_\theta^*, \lambda^*\right). \tag{17}$$

We define a brachiation fixed point as a solution (x_θ^*, λ^*) to (17) such that b^+ corresponds to the double pendulum mode.

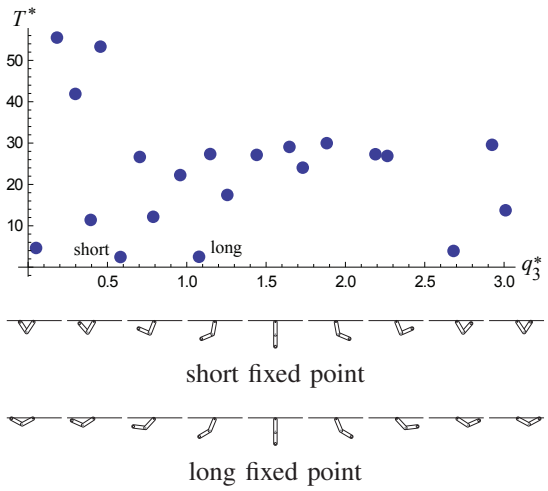

Fig. 5: Several Gomes-Ruina fixed points in the (q_3^*, T^*) plane, and two solutions shown as animations.

D. The Gomes-Ruina Fixed Points

Some solutions of (17) do not require any torque throughout the swing motion. A subset of these solutions impact with zero velocity at time T^* in a configuration mirroring the original stationary configuration. These are the zero-energy horizontal brachiation fixed points identified for the symmetric brachiator by Gomes and Ruina (Figure 5). These solutions are fully specified by q_3^*, T^*, and zero control torque. We refer to these fixed points as Gomes-Ruina fixed points (or GR fixed points). An important consequence of zero impact velocity and zero energy input is that all GR fixed points are unstable. In the next section we explore stable fixed points of (16) that have non-zero velocity impacts.

In our search for stable gaits, we used the same physical parameters used by Gomes and Ruina for their two link brachiator model. The nondimensionalized parameters for their system are approximately

$$\alpha = 38.263 \quad \beta = 18.132 \quad \delta_1 = 0.5 \quad \delta_2 = 0.5$$
$$\gamma = 1 \quad \kappa_1 = 0.277 \quad \kappa_2 = 8.843.$$

IV. Passive Downhill Brachiation

The GR solutions are unstable, as energy dissipation is necessary for stability. For periodic motion, this energy must be replenished. By brachiating downhill, similar to an upside-down compass gait walker [5], [6], in each cycle the Gibbot converts some potential energy to kinetic energy, and then dissipates the same amount of energy on impact. To create this downhill brachiation, we switch the magnets when the hands lie on a sloped line as seen in Figure 6. The slope that the Gibbot brachiates on has an angle $\sigma > 0$ from the slope to the horizontal.

We would like to find the stable and unstable period-one fixed points for passive downhill brachiation. These post-impact fixed points lie in a four-dimensional $(\sigma, q_4, \dot{q}_3, \dot{q}_4)$ space. (Note that the slope angle σ and q_4 uniquely define q_3 just after impact.) We will find it convenient to represent the post-impact configuration on the slope by the *interleg angle* $\nu = \pi - q_4$, illustrated in Figure 6. Thus our search for fixed points is in the four-dimensional $(\sigma, \nu, \dot{q}_3, \dot{\nu})$ space, which we call $\mathcal{M}$.

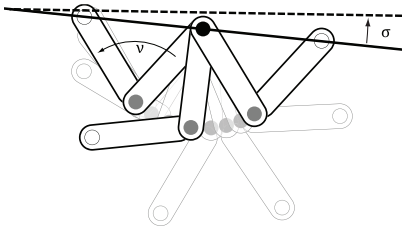

Fig. 6: An example of passive stable downhill brachiation on a slope of $\sigma = 0.1$ radians and an interleg angle of $\nu = 1.287$ radians.

The unstable "short" and "long" GR solutions, illustrated in Figure 5, are isolated points in the four-dimensional space $\mathcal{M}$, at $\nu = 1.16$ radians for the short solution, $\nu = 2.15$ radians for the long solution, and $\sigma = \dot{q}_3 = \dot{\nu} = 0$ for both. The idea is to use these solutions as starting points and apply continuation methods to search for the existence of nearby fixed points in $\mathcal{M}$ where $\sigma > 0$, corresponding to downhill brachiation. (There can be no passive fixed points for $\sigma < 0$; actuated, but open-loop, fixed points are considered in Section V. These two GR solutions are the shortest-duration and simplest brachiation motions, and therefore the most likely prototypes for stable open-loop uphill brachiation.) We limit our study to a neighborhood of these two solutions and do not attempt to fully understand the topology of the fixed points in $\mathcal{M}$. See Figure 5 for an idea of the complexity.

Our results are summarized in Figure 7, which is a projection of $\mathcal{M}$ onto the (σ, ν) space. The projections of the GR solutions are indicated by asterisks. Starting from the unstable long GR solution, we increase σ slightly to $\sigma + \delta$ and use an optimization-based continuation method to find a nearby point $(\sigma + \delta, \nu, \dot{q}_3, \dot{\nu})$ satisfying the fixed-point condition (17). This new point is the initial guess to find a next fixed point at $\sigma + 2\delta$, etc. This method shows that the long GR solution belongs to a one-dimensional family of fixed points extending to downhill slopes up to approximately $\sigma = 0.14$ radians, or 8 degrees. This family is denoted A in Figure 7. These fixed points are stable in the range $0.005 < \sigma < 0.128$.

We also found a family B of unstable fixed points running from slopes of approximately $\sigma = 0.01$ radians to $\sigma = 0.43$ radians. This family appears to connect to the short GR solution, but we were unable to verify this definitively.

Finally, we found one other nearby solution family C that does not appear to be connected to a GR fixed point. This family C extends from $\sigma = 0.035$ radians to beyond $\sigma = 0.5$ radians, and includes stable fixed points from $\sigma = 0.035$ radians to $\sigma = 0.435$ radians.

Figure 8 plots the magnitude of the maximum eigenvalue of the return map S corresponding to points in family C. According to this measure, passive downhill brachiation is

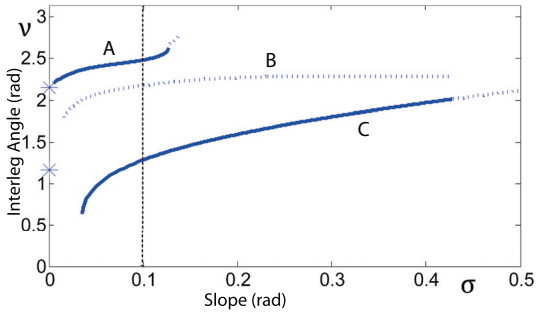

Fig. 7: Fixed-point families A, B, and C projected to (σ, ν). Solid lines indicate stable fixed points and dashed lines indicate unstable. Asterisks at zero slope indicate GR solutions. The dotted vertical line at a slope of 0.1 radians indicates the slice shown in Figure 9.

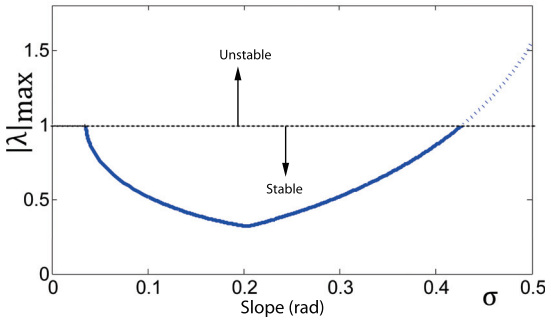

Fig. 8: The magnitude of the largest eigenvalue of the return map S of family C fixed points, plotted as a function of slope.

most stable at a slope of $\sigma = 0.2$.

Figure 9 plots the basins of attraction of the family A "long" interleg angle stable fixed points and the family C "short" stable fixed points in the two-dimensional slice $\{\mathcal{M} \mid \sigma = 0.1, \dot{q}_3 = 0\}$. Each point in this slice converges to a stable A or C fixed point. Thus the basins of attraction of the two stable fixed-point families are quite large (and appear to partition the entire $(\nu, \dot{\nu})$ space), unlike the fixed points of the Gibbot's inverted counterpart, the compass-gait walker. Also unlike the compass-gait walker, we did not observe period-doubling bifurcations in brachiation gaits at steep slopes where the stable period-one solutions disappear.

Because of the large basins of attraction of the stable fixed points of familes A and C, these fixed points are easy to find through simulation. Our simulations confirm that the stable fixed points are disconnected one-dimensional curves in $\mathcal{M}$. For all initial conditions we tried, the Gibbot converged either to a stable point in A, a stable point in C, or never converged at all. We did not observe other periodic or quasi-periodic gaits.

By a counting argument, we hypothesize that the families A, B, and C, including the unstable fixed points, are one-dimensional sets. The fixed-point condition places three constraints on the four variables in $\mathcal{M}$, generically resulting

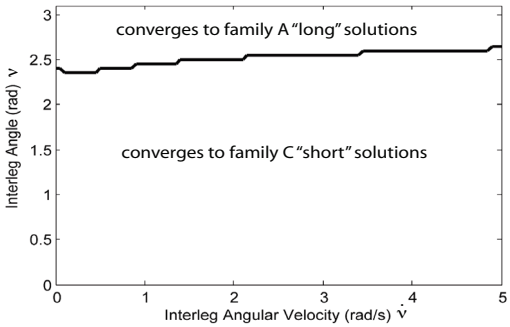

Fig. 9: Basins of attraction for family A and family C stable fixed points for a slope of $\sigma = 0.1$ radians and $\dot{q}_3 = 0$.

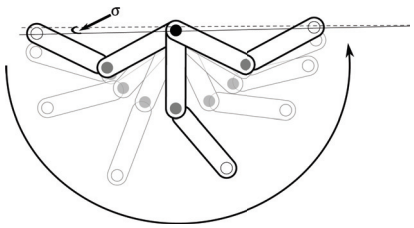

Fig. 10: An example of an actuated uphill brachiation on a slope of 0.024 radians.

in one-dimensional solution sets. Figure 9 is indicative of a three-dimensional unstable surface separating families A and C, which we see as a line in the projection of the figure.

Finally, by analogy to the compass-gait walker, in this section we assumed that the free-swinging magnet activates upon reaching the virtual slope. While this happens mechanically for the walker, the Gibbot requires a sensor to implement this switch. To eliminate this sensor, we also considered the case where the Gibbot switches the magnets according to a time schedule. Preliminary tests show that stable solutions shown above remain stable under this alternate time-based switching strategy. Thus passive downhill brachiation can be both stable and sensorless. In the next section, we investigate a time-based switching strategy for powered, but still sensorless, uphill brachiation.

V. Uphill Stable Brachiation

One limitation of the passive brachiating solutions is that the continuous contact gaits can only brachiate downhill. We can overcome this limitation by powering the motor for which we choose the simplest forcing function, $u(t) = u > 0$. An example of an uphill brachiating fixed point is shown in Figure 10. This particular fixed point is part of a family of uphill climbing solutions that extend from the long GR solution, which has an initial configuration of $(q_3^*, q_4^*) \approx (-1.077, -0.987)$ and switching time $T^* \approx 2.508$. The initial condition x_θ^*, torque u^*, and switching time T^* for the uphill climbing gait are approximately

$$x_\theta^* = \begin{bmatrix} -1.065, & -0.964, & 0.044, & -0.007 \end{bmatrix}^T, \\ u^* = 0.451, \quad T^* = 2.514. \tag{18}$$

The fixed point is stable (as illustrated in Figure 11) with a maximum eigenvalue of about 0.95. In our numerical simu-

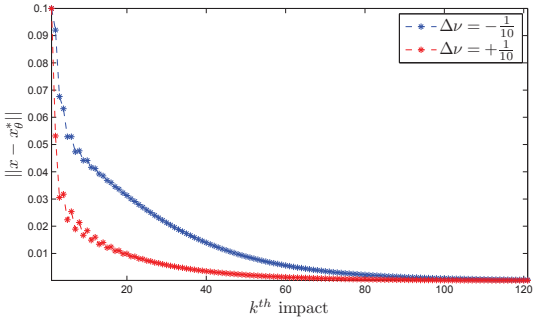

Fig. 11: The normed error between the uphill fixed point and the post-impact state due to small perturbations of $\pm\frac{1}{10}$ radian to the interleg angle ν at $t = 0$.

lations we find several families of fixed points parametrized by the controls, where the special case of $u = 0$ corresponds to a Gomes Ruina solution. Unlike the GR solutions, our climbing solutions are sometimes stable, and unlike existing control strategies for brachiation that we have found in the literature, our method is open-loop.

In our simulations we have found stable downhill and uphill motions of varying periodicity, but with only one torque and switching time for controls we are limited in the nearby fixed points we can reach from a GR solution. We can show that if we break $u(t)$ into a piecewise-constant function comprised of three constant torques that, along with the final switching time, we can locally reach a full dimensional subset of fixed points near a GR solution. Because of space constraints we cannot show the derivation, but in future work we plan to utilize the result for planning more complicated motions besides the ones presented in this paper.

VI. Conclusions and Future Work

We have shown that unstable, zero-energy brachiating solutions serve as natural templates for stable brachiation with or without control. In a future paper, we plan to expand on our numerical results. For example, our simulations show that the long Gomes-Ruina solution was capable of producing stable locomotion for passive descent and controlled ascent, i.e., open-loop control destabilized the passive gait. Controlled descent was the only stable locomotion produced by the short solution, i.e., open-loop control stabilized the unstable passive motion. These results suggest that the long zero-energy solution is more useful as a motion template for brachiating in arbitrary directions. Future work will verify these observations experimentally.

We noticed several differences between passive brachiation and previous results on passive walking. We found two families of stable brachiating solutions over a range of slope angles, whereas only one family of stable walking solutions has been reported in the literature [5], [6]. Neither stable family exhibited period-doubling behavior on extreme slope angles, whereas a period-doubling cascade into chaos has been documented for the compass-gait biped [6]. Although this paper did not examine regions of attraction in-depth, the stable brachiating gaits were attractive for a large range of initial conditions. This suggests that the region of attraction for passive brachiating may be significantly larger than for passive walking, which is known to be sensitive to initial conditions. We leave this robustness analysis to future work.

This paper motivates further study of the Gibbot, which is capable of other forms of locomotion. Our model can transition into free-flight dynamics during swing phase to allow fast *ricochetal* brachiation. We are also interested in analyzing period-two (asymmetric) locomotor patterns. By employing a diverse suite of gaits, the Gibbot will be able to perform gymnastic maneuvers to reach specific handholds in the environment. Future work will use motion planning approaches based on asymptotically stable primitives [16] or optimization [17] to generate paths composed of these dynamic motions.

References

[1] F. Saito, T. Fukuda, and F. Arai, "Swing and locomotion control for a two-link brachiation robot," *IEEE Control Systems Magazine*, vol. 14, no. 1, pp. 5–12, 1994.

[2] J. Nakanishi, T. Fukuda, and D. Koditschek, "A brachiating robot controller," *IEEE Trans. Robotics & Automation*, vol. 16, no. 2, pp. 109–123, 2000.

[3] T. Fukuda, M. Doi, Y. Hasegawa, and H. Kajima, "Multi-locomotion control of biped locomotion and brachiation robot," in *Fast Motions in Biomechanics and Robotics*, ser. Lecture Notes in Control and Information Sciences. Heidelberg, Allemagne, Germany: Springer, 2006, pp. 121–145.

[4] M. W. Gomes and A. L. Ruina, "A five-link 2D brachiating ape model with life-like zero-energy-cost motions," *J. Theoretical Biology*, vol. 237, pp. 265–278, 2005.

[5] M. Garcia, A. Chatterjee, A. Ruina, and M. Coleman, "The simplest walking model: Stability, complexity, and scaling," *ASME J. Biomechanical Engineering*, vol. 120, no. 2, pp. 281–288, 1998.

[6] A. Goswami, B. Thuilot, and B. Espiau, "A study of the passive gait of a compass-like biped robot: Symmetry and chaos," *Int. J. Robotics Research*, vol. 17, no. 12, pp. 1282–1301, 1998.

[7] S. H. Collins and A. L. Ruina, "A bipedal walking robot with efficient and human-like gait," in *IEEE Int. Conf. on Robotics and Automation*, Barcelona, Spain, 2005, pp. 1983–1988.

[8] M. W. Spong and F. Bullo, "Controlled symmetries and passive walking," *IEEE Trans. Automatic Control*, vol. 50, no. 7, pp. 1025–1031, 2005.

[9] R. D. Gregg and M. W. Spong, "Reduction-based control of three-dimensional bipedal walking robots," *Int. J. Robotics Research*, vol. 26, no. 6, pp. 680–702, 2010.

[10] F. Bullo and M. Zefran, "Modeling and controllability for a class of hybrid mechanical systems," *IEEE Trans. Robotics & Automation*, vol. 18, no. 4, pp. 563–573, 2002.

[11] M. W. Spong, "The swing up control problem for the Acrobot," *IEEE Control Systems Magazine*, vol. 15, no. 1, pp. 49–55, 1995.

[12] W. R. Provancher, S. I. Jensen-Segal, and M. A. Fehlberg, "ROCR: An energy-efficient dynamic wall-climbing robot," *IEEE/ASME Trans. Mechatronics*, no. 99, p. 10.

[13] A. Mazumdar and H. H. Asada, "An underactuated, magnetic-foot robot for steel bridge inspection," *ASME J. Mechanisms & Robotics*, vol. 2, no. 3, 2010.

[14] F. Rochat, P. Schoeneich, M. Bonani, S. Magnenat, F. Mondada, and H. Blueler, "Design of magnetic switchable device (MSD) and applications in climbing robot," in *CLAWAR*, 2010.

[15] E. Allgower and K. Georg, *Numerical Continuation Methods, An Introduction*. New York, NY: Springer-Verlag New York, Inc., 1990.

[16] R. D. Gregg, T. W. Bretl, and M. W. Spong, "Asymptotically stable gait primitives for planning dynamic bipedal locomotion in three dimensions," in *IEEE Int. Conf. on Robotics and Automation*, Anchorage, AK, 2010, pp. 1695–1702.

[17] A. W. Long, T. D. Murphey, and K. M. Lynch, "Optimal motion planning for a class of hybrid dynamical systems with impacts," in *IEEE Int. Conf. Robotics & Automation*, 2011, pp. 4220–4226.